**FACTA UNIVERSITATIS**
Series: **Electronics and Energetics** Vol. 30, N$^{o}$ 4, December 2017, pp. 431 - 458
DOI: 10.2298/FUEE1704431M

# DESIGN OF MICROWAVE WAVEGUIDE FILTERS WITH EFFECTS OF FABRICATION IMPERFECTIONS

**Marija Mrvić, Snežana Stefanovski Pajović, Milka Potrebić, Dejan Tošić**

University of Belgrade, School of Electrical Engineering, Belgrade, Serbia

**Abstract**. *This paper presents results of a study on a bandpass and bandstop waveguide filter design using printed-circuit discontinuities, representing resonating elements. These inserts may be implemented using relatively simple types of resonators, and the amplitude response may be controlled by tuning the parameters of the resonators. The proper layout of the resonators on the insert may lead to a single or multiple resonant frequencies, using single resonating insert. The inserts may be placed in the E-plane or the H-plane of the standard rectangular waveguide. Various solutions using quarter-wave resonators and split-ring resonators for bandstop filters, and complementary split-ring resonators for bandpass filters are proposed, including multi-band filters and compact filters. They are designed to operate in the X-frequency band and standard rectangular waveguide (WR-90) is used. Besides three dimensional electromagnetic models and equivalent microwave circuits, experimental results are also provided to verify proposed design. Another aspect of the research represents a study of imperfections demonstrated on a bandpass waveguide filter. Fabrication side effects and implementation imperfections are analyzed in details, providing relevant results regarding the most critical parameters affecting filter performance. The analysis is primarily based on software simulations, to shorten and improve design procedure. However, measurement results represent additional contribution to validate the approach and confirm conclusions regarding crucial phenomena affecting filter response.*

**Key words**: *bandpass filter, bandstop filter, multi-band filter, printed-circuit discontinuity, equivalent circuit, fabrication effects*

## 1. INTRODUCTION

A great diversity of microwave filters can be perceived in modern communication systems. Continuous improvement of these systems needs microwave filters having much more features such as low cost, compact size, low loss and operation in several frequency bands. Therefore, this topic still gains significant attention in the area of microwave engineering.

Received February 18, 2017
**Corresponding author:** Marija Mrvić
School of Electrical Engineering, University of Belgrade, Kralja Aleksandra Blvd. 73, 11120 Belgrade, Serbia
(E-mail: marija.mrvic@gmail.com)

A filter design procedure consists of several steps, which assume specification, approximation, synthesis, simulation model, implementation, study of imperfections and optimization [1, 2]. The purpose of each step can be briefly explained as follows [3]. Design starts by setting the criteria (a filter specification) to be met for potential application. Specification should be mathematically represented, so we need an approximation which is actually a filter transfer function. At that point filter simulation model and filter prototype (a fabricated device) may be introduced and evaluated. Study of imperfections is then performed to investigate the various effects and phenomena caused by the real components used for the filter implementation. Finally, optimization may be used for systematic numerical tuning of filter parameters to meet the specification.

Amongst the available filter manufacturing technologies, rectangular waveguides are attractive in communication systems, such as radar and satellite systems, due to their ability to handle high power and have low losses [4]. In this technology, bandstop and bandpass filters can be easily implemented with properly employed feeders [5]. Filters are designed by inserting discontinuities into the *E*-plane or *H*-plane of the rectangular waveguides. Various types of resonators, in relatively simple forms to design and fabricate, can be used on these discontinuities to obtain resonating inserts with a single or multiple resonant frequencies. For the *E*-plane filters, it is important to properly couple the resonators of the same frequency, and to decouple the resonators operating at the different frequencies. On the other hand, for the *H*-plane filters, it is important to decouple the resonators with the different resonant frequencies on the same insert, and to properly implement the inverters between the resonators with the same resonant frequency [6].

In this paper, various types of bandstop and bandpass waveguide filters, with single or multiple frequency bands, are presented and their characteristics are analyzed in details. The proposed filters are designed to operate in the X frequency band (8.2–12.4 GHz); therefore standard rectangular waveguide WR-90 (inner cross-section dimensions: width $a$ = 22.86 mm, height $b$ = 10.16 mm) is used and the dominant mode of propagation $TE_{10}$ is considered. Both *E*-plane and *H*-plane filters are presented. Split-ring resonators (SRRs) and quarter-wave resonators (QWRs) are used for the bandstop, and complementary split-ring resonators (CSRRs) for the bandpass filter design. Along with the three-dimensional electromagnetic (3D EM) models, equivalent microwave circuits are generated and, for the chosen examples, the obtained results are also experimentally verified. Bearing in mind the operational frequency band and implementation technology, these filters can be used as components of radar and satellite systems of various purposes [3].

A study of imperfections, based on the fabrication side effects investigation, is also presented and exemplified. A waveguide resonator and a third-order bandpass waveguide filter are analyzed in details in terms of implementation imperfections, including: implementation technology, the tolerance of the machine used for fabrication and positioning of the inserts inside the waveguide. This investigation provided relevant results regarding the most critical parameters influencing the filter performance. It is based on the software simulations, thus shortening and improving design procedure, and verified by the measurements on a laboratory prototype.

## 2. BANDSTOP FILTER DESIGN

Bandstop filters, as key components in RF/microwave communication systems, have an important task to reject the unwanted signals [7]. They can be easily implemented by inserting discontinuities into the *E*-plane or *H*-plane of the rectangular waveguides. Authors in [8] present the *H*-plane filter using horizontal and vertical stepped thin wire conductors connecting the opposite waveguide walls. The usefulness of the SRRs is verified for compact waveguide *H*-plane filter design in [9-13] and for the *E*-plane filter design in [14-17].

In this section, *E*-plane and *H*-plane bandstop waveguide filters are discussed. Both types of filters use printed resonators as QWRs and SRRs. Compact size and independent control of the designed stopbands is a common feature of presented filters. For both of them, independently tunable stopbands are achieved in diverse manners, so detailed design procedures and results are presented.

### 2.1. *E*-plane bandstop waveguide filters using QWRs

*E*-plane single-band filter design using QWRs, presented in [18], is expanded for the multi-band bandstop filter design [19]. First, we consider waveguide QWR, shown in Fig. 1a, designed for resonant frequency $f_0$ = 11 GHz. Presented QWR is printed on the upper side of the substrate and connected to the lower waveguide wall.

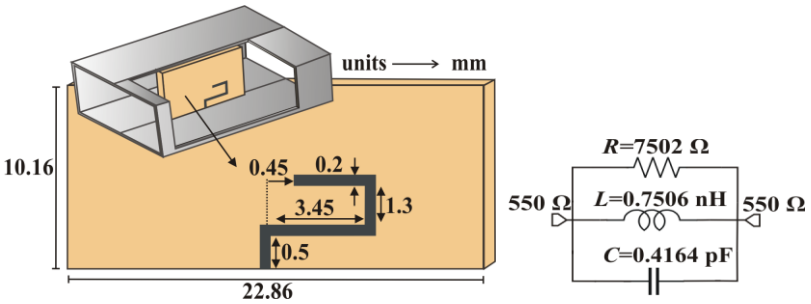


(a)

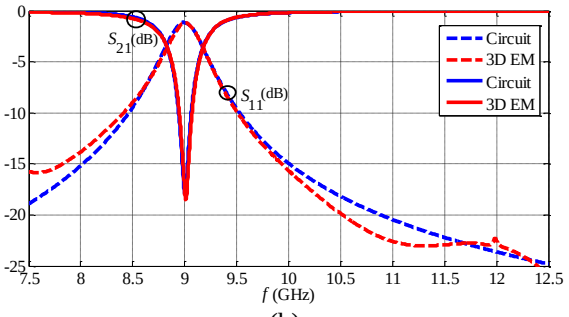


(b)

**Fig. 1** a) Waveguide QWR: 3D model and equivalent circuit, b) comparison of amplitude responses for the 3D model and equivalent electrical circuit of the QWR

Fiberglass/PTFE resin laminate (TLE-95) (www.taconic-add.com) is chosen as a substrate to implement the *E*-plane inserts. The parameters of the substrate are: $\varepsilon_r = 3$, $h = 0.11176$ mm, $\tan\delta = 0.0028$, $t = 0.0175$ mm. The metal losses due to the skin effect and surface roughness are taken into account by setting the conductivity $\sigma = 20$ MS/m.

The equivalent-circuit model of the waveguide QWR is shown in Fig. 1a. Simulated results for the 3D EM model of the waveguide QWR and its equivalent circuit are compared in Fig. 1b. The values of the circuit elements are calculated using equation (1), as proposed in [6]:

$$R = 2Z_0 \frac{|S_{11}(j\omega_0)|}{1-|S_{11}(j\omega_0)|},\ L = 2B_{3dB}Z_0 \frac{|S_{11}(j\omega_0)|}{\omega_0^2},\ C = \frac{1}{2B_{3dB}Z_0|S_{11}(j\omega_0)|}, \tag{1}$$

where $\omega_0$ denotes the angular frequency in (rad/s), $B_{3dB}$ is 3dB bandwidth (rad/s), $S_{11}(j\omega_0)$ is the value of the $S_{11}$ parameter at the considered resonant frequency. The impedances of ports correspond to the value of the wave impedance of the waveguide for the resonant frequency of $f_0 = 9$ GHz (550 Ω).

Quality factor (*Q*-factor) is an important parameter that characterizes a microwave resonator. Detailed determination of the *Q*-factor for the considered resonator is given in [19]. The obtained Q-factors are $Q_L = 22.5$ for the loaded resonator, and $Q_U = 175.34$ for the unloaded resonator.

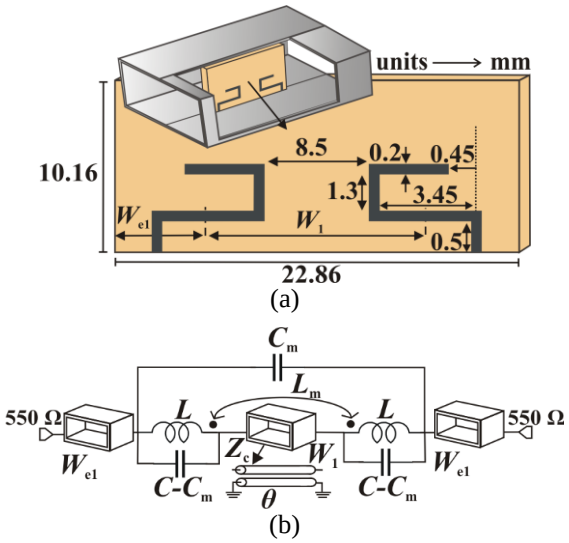


**Fig. 2** *E*-plane waveguide bandstop filter a) 3D model, b) equivalent microwave circuit

*2.1.1. Bandstop waveguide filter and equivalent circuit*

Bandstop waveguide filter using presented QWRs is shown in Fig. 2a. A printed-circuit insert consisting of two identical QWRs is placed in the *E*-plane of the rectangular waveguide. Center frequency of the bandstop filter can be targeted by adjusting the length of the used QWRs. QWRs are grounded to the lower waveguide wall and the spacing

between them yields the desired bandwidth. For the considered filter, the center frequency is $f_0$ =9 GHz and QWRs are spaced 8.5 mm apart to achieve the bandwidth of 570 MHz.

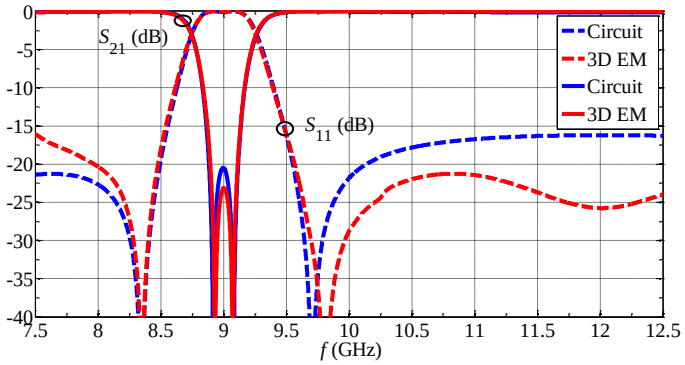


**Fig. 3** Comparison of amplitude responses for the bandstop filter (Fig. 2a) and its equivalent circuit (Fig. 2b)

Equivalent circuit of the bandstop waveguide filter using QWRs is shown in Fig. 2b. To develop equivalent circuit, QWRs are represented using mutually coupled *LC* resonators. The coupling is composed of the following elements: inductor ($L_m$) provides the magnetic part of the coupling and capacitor ($C_m$) provides electric part of the coupling. Values of $L$ and $C$ are found from equation (1). The waveguide section of length $W_1$ comprises the distance between middle parts of the QWRs in 3D EM model, and in calculations, it was replaced by the equivalent transmission line of characteristic impedance $Z_c = 550\ \Omega$, and electrical length $\theta = 1.60$ rad at 9 GHz. Having determined all these parameters, we can find the values of the coupling elements ($L_m$, $C_m$) using equation (2):

$$f_1 = \frac{2(L-L_m)\cot\left(\frac{\theta}{2}\right)+\sqrt{2}\csc\left(\frac{\theta}{2}\right)\sqrt{L-L_m}\sqrt{L-L_m+4(C-C_m)Z_c^2+(L-L_m+4(-C+C_m)Z_c^2)\cos(\theta)}}{4(L-L_m)(C-C_m)Z_c}$$

$$f_2 = \frac{-(L+L_m)\tan\left(\frac{\theta}{2}\right)+\sqrt{(L+L_m)\left(4(C-C_m)Z_c^2+(L+L_m)\tan\left(\frac{\theta}{2}\right)^2\right)}\Big/\operatorname{sign}\left(\cos\left(\frac{\theta}{2}\right)\right)}{2(L+L_m)(C-C_m)Z_c}. \quad (2)$$

This equation is derived for the resonant frequencies ($f_1$, $f_2$) of the coupled QWRs. The numeric values of these resonant frequencies are found for unloaded coupled resonators in the 3D EM model. Values of the circuits elements are, as follows: $L$ = 0.757 nH, $L_m$ = 0.00371 nH, $C$ = 0.4136 pF, $C_m$ = 0.00038 pF, $W_1$ = 12.35 mm and $W_{e1}$ = 5.255 mm. Fig. 3. shows the comparison of simulated amplitude responses for the 3D EM and equivalent circuit model of the waveguide bandstop filter.

*2.1.2. Multi-band bandstop waveguide filter design*

To validate the design of the *E*-plane waveguide filters with multiple stopbands, filters with two and three stopbands are designed. Presented filters exhibit independent control of the designed stopbands (ICDS).

3D models of the non-miniaturized ICDS (nmICDS) and miniaturized (mICDS) dual-band bandstop waveguide filters are shown in Fig. 4. Specified center frequencies of the dual-band bandstop filter are $f_{01}$ = 9 GHz and $f_{02}$ = 11 GHz. As for the nmICDS dual-band filter design, all of the printed QWRs are connected to the same waveguide wall.

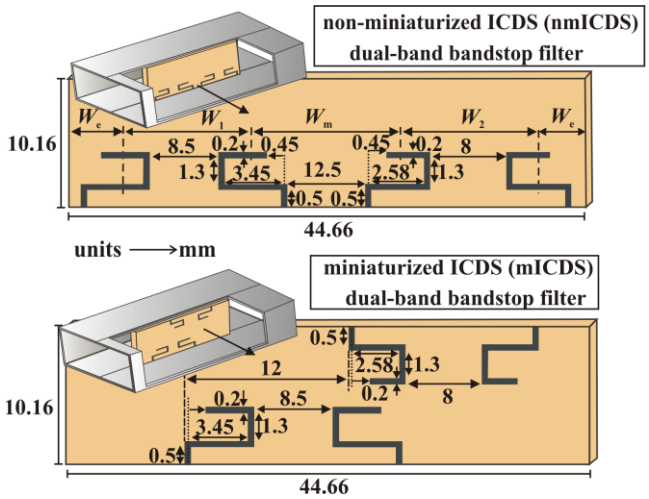


**Fig. 4** 3D models of the nmICDS and mICDS *E*-plane dual-band waveguide filters

To eliminate the unwanted coupling between the QWRs for different stopbands, they are separated far from each other by the spacing of 12.5 mm. In that manner, each of the stopbands can be controlled individually, and the whole filter is perceived as a cascade connection of the bandstop filters intended for particular stopband performance. Overall length of the nmICDS filter is 0.876 $\lambda_g$, where $\lambda_g$ denotes the guided wavelength at the center frequency of the lower stopband.

With the aim to reduce the footprint of the nmICDS filter, QWRs for different stopbands are connected to the different waveguide walls, which is in fact relatively simple solution to implement mICDS dual-band bandstop waveguide filter. Amplitude responses of the nmICDS and mICDS filters exactly match. For the mICDS filter, the unwanted coupling is overcome by shifting the QWRs for specified stopband along the upper waveguide wall. It was found that minimal value of the shift is 12 mm. However, the overall length decreased to 0.512 $\lambda_g$.

Equivalent microwave circuit of the nmICDS dual-band bandstop filter is the cascade of the equivalent networks of single-band filters (Fig. 2b) with the specified center frequencies, and it is shown in Fig. 5a. The ports impedances are set to 500 Ω, which is the value adequate for the wave impedance at 10 GHz (frequency in the middle of the considered center frequencies). The values of the equivalent circuit elements of the filter at 9 GHz remain unchanged, while circuit elements' values for the filter at 11 GHz are:

$L_2$ = 0.518 nH, $L_{m2}$ = 0.001122 nH, $C_2$ = 0.4036 pF, $C_{m2}$ = 0.0007 pF, $W_2$ = 10.98 mm, $W_m$ = 15.92 mm and $W_e$ = 2.705 mm. Amplitude responses of the 3D EM model and its equivalent circuit are compared in Fig. 5b.

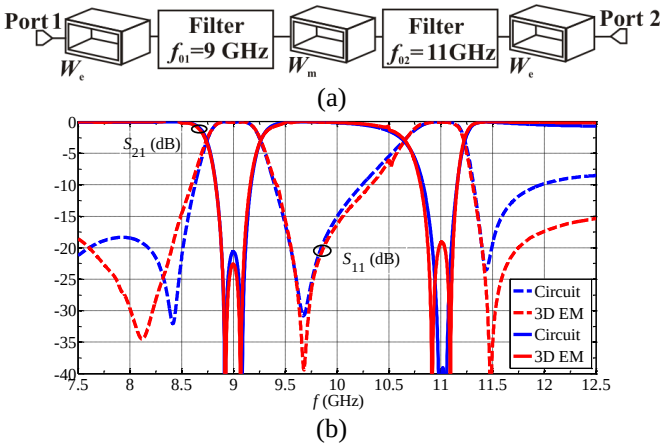


**Fig. 5** a) Equivalent microwave circuit of the nmICDS filter from Fig. 4. b) Comparison of amplitude responses for the 3D EM model of the nmICDS filter and its equivalent circuit

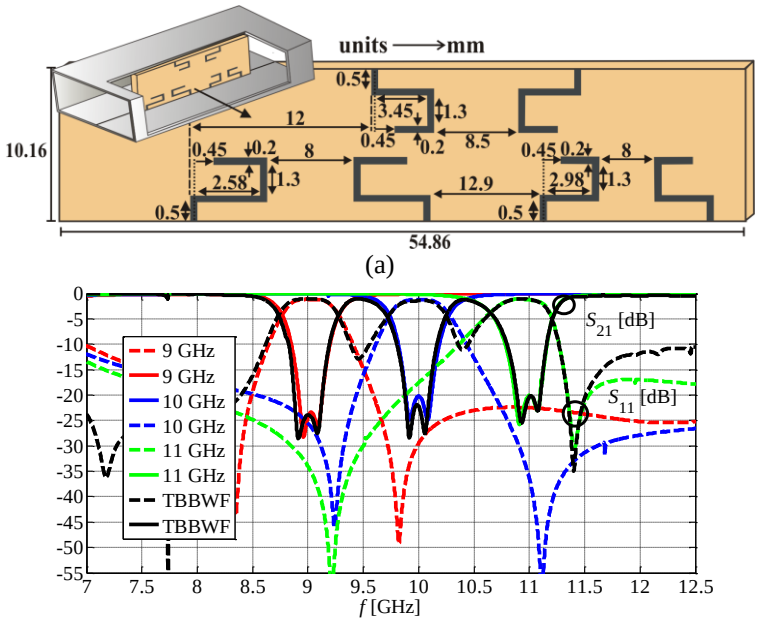


**Fig. 6** a) TBBWF b) Comparison of amplitude responses for the ICDS TBBWF and single-band filters for each specified center frequency

According to the proposed design guidelines, triple-band bandstop waveguide filter (TBBWF) is designed for specified center frequencies $f_{01}$ = 9 GHz, $f_{02}$ = 10 GHz and $f_{03}$ = 11 GHz. Middle stopband is designed by adding pair of identical QWRs having their length tuned to resonate at $f_0$ = 10 GHz. So, TBBWF consists of alternating pairs of QWRs for different stopbands, attached to the top and bottom waveguide walls. 3D model of the TBBWF is shown in Fig. 6a. The proposed design of the filter with three stopbands assumes that QWRs for the second and third stopband are connected to the same waveguide wall, while the QWRs for the first stopband are grounded to the opposite waveguide wall. The distances between the QWRs are set to secure the independent control of the stopbands. Comparison of amplitude responses for the TBBWF and single-band filters for each specified center frequency is given in Fig. 6b. Total length of the TBBWF is 0.86 $\lambda_g$, $\lambda_g$ being the guided wavelength at the lowest center frequency.

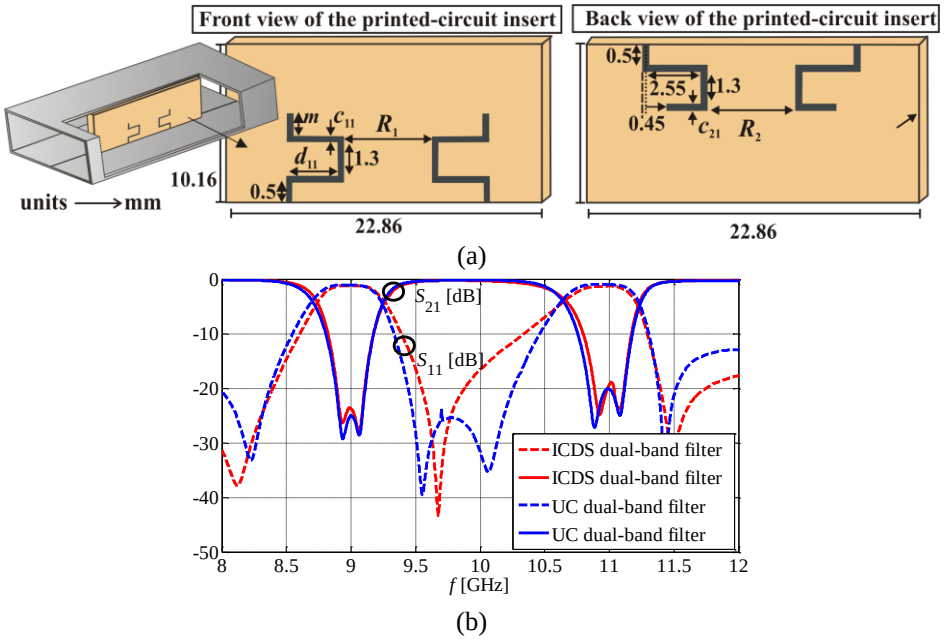


**Fig. 7** a) 3D model of the UC dual-band bandstop waveguide filter. b) Comparison of simulated amplitude responses for the UC and ICDS dual-band waveguide filters

*2.1.3. Miniaturization*

Further miniaturization of the mICDS dual-band bandstop filter is achieved through several steps. 3D model of the presented ultra-compact (UC) dual-band bandstop filter is shown in Fig. 7a. Some of the geometric parameters are given symbolically to investigate their impact on the filter response. QWRs for different stopbands are printed on different sides of the insert. The aim was to preserve the characteristics of the mICDs filter, but to reduce the length of the filter. The whole length of the UC dual-band bandstop filter is 0.295 $\lambda_g$. The proximity of the participating QWRs restricted the independent control of the stopbands. Comparison of simulated amplitude responses for the UC and ICDS dual-

band bandstop waveguide filters is shown in Fig. 7b. The effect of the alterations of the parameters on the center frequencies and obtained bandwidths is exposed in Table 1.

**Table 1** Influence of the parameters on the response of the UC dual-band filter

| Parameter in (mm) | $f_{01}$ (GHz) | $B_{3dB1}$ (MHz) | $f_{02}$ (GHz) | $B_{3dB2}$ (MHz) |
|---|---|---|---|---|
| $c_{21}$ ↑ | – | – | ↓ | ↑ |
| $c_{11}$ ↓ | ↓ | ↓ | ↓ | ↑ |
| $R_2$ ↓ | – | ↓ | – | ↑ |
| $R_1$ ↓ | ↑ | ↑ | ↓ | ↑ |
| $d_{11}$ ↑ | ↓ | ↑ | – | ↑ |
| $m$ ↑ | ↑ | ↑ | – | ↓ |

Possibilities regarding further miniaturization included the straight form of the QWRs and variation in the increment of the dielectric constant of the substrate used for implementation of the QWRs. The filter design with QWRs in the straight form features significantly wider bandwidths compared to the case when QWRs are implemented as folded elements. So, to preserve the characteristics of the ICDS filter, the space between the QWRs should be increased, resulting in longer filter than mICDS. The same effect is observed for substrates with higher permittivity ($\varepsilon_r$). Since the higher $\varepsilon_r$ makes the length of the printed QWRs shorter, the bandwidth became significantly wider. So, we had to increase the distance between the QWRs, which in turn increases the length of the filter. As a consequence, that filter is longer than our proposed realization. Additional solution for miniaturization is proposed in [20], where connection of the QWRs for specified stopband to the opposite waveguide walls is suggested.

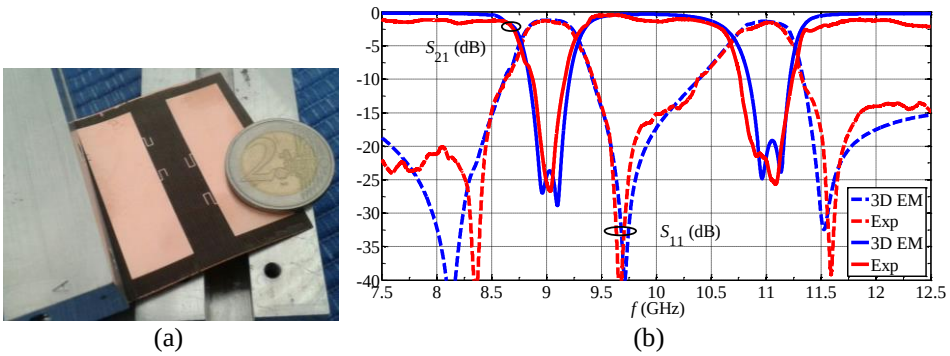


(a) (b)

**Fig. 8** a) A photograph of the fabricated *E*-plane dual-band bandstop waveguide filter. b) Comparison of the simulated and measured results

*2.1.4. Experimental verification*

In order to demonstrate the effectiveness of the proposed design, the *E*-plane dual-band bandstop filter is verified on a fabricated prototype (Fig. 8a). The amplitude response was measured using Agilent N5227 network analyzer. Fig. 8b shows comparison between the measured and simulated amplitude responses for the dual-band bandstop

filter. Measured response is in good agreement with the 3D EM simulation results. Slight discrepancies are observed in terms of the passband insertion loss, which occurred as a consequence of the losses within the waveguide walls and transitions from waveguide WR-90 to SMA connectors (waveguide-to-coaxial adapters). These losses have not been taken into account during the 3D EM analysis of the considered filter.

### 2.2. *H*-plane bandstop waveguide filters using SRRs

For the implementation of the *H*-plane filter, SRRs in the form of the printed-circuit inserts are positioned in the transverse plane of the standard WR-90 waveguide [11, 12]. The printed-circuit inserts are implemented using copper clad PTFE/woven glass laminate (TLX-8) with the parameters: $\varepsilon_r = 2.55$, $\tan\delta = 0.0019$, $h = 1.143$ mm and $t = 0.018$ mm. The losses due to the skin effect and surface roughness are taken into account by setting the conductivity to $\sigma = 20$ MS/m.

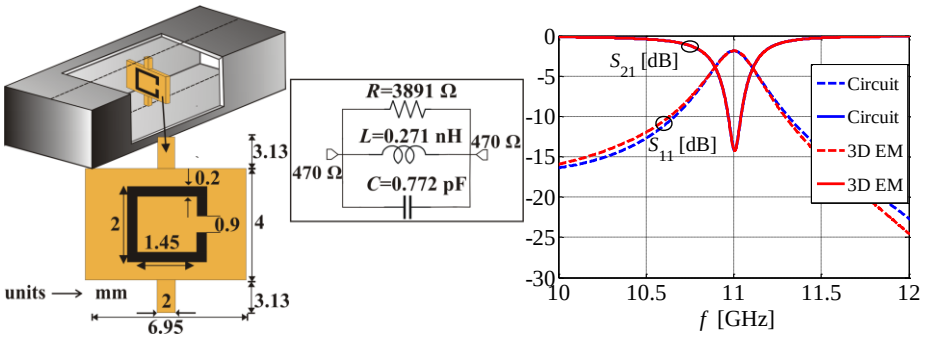


(a) (b)

**Fig. 9** SRR: a) 3D and equivalent circuit model. b) Comparison of amplitude responses

#### *2.2.1. Waveguide SRR*

3D model of the considered *H*-plane waveguide SRR is presented in Fig. 9a. It is designed for resonant frequency of 11 GHz, so appropriate dimensions are given. Equivalent circuit model is also presented in Fig. 9a, and the values of the circuits' elements are obtained using the equation (1). Comparison of amplitude responses for the 3D EM model and its equivalent circuit is shown in Fig. 9b.

#### *2.2.2. Third-order bandstop waveguide filter using SRRs*

A third-order bandstop waveguide filter using SRRs is designed for the center frequency $f_0 = 11$ GHz [11, 12]. 3D model of the filter is shown in Fig. 10a, and its response is given in Fig 10b. The *H*-plane inserts are separated by the waveguide section of length of $\lambda_{g11GHz}/4 = 8.494$ mm, to implement the quarter-wave inverters for the center frequency.

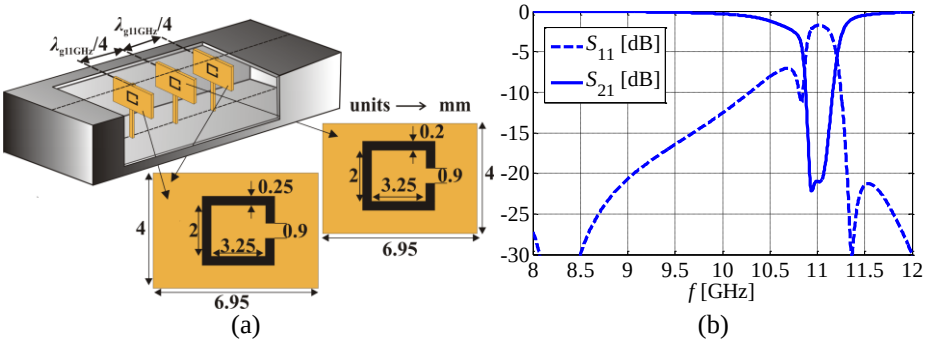


**Fig. 10** *H*-plane bandstop filter using SRRs: a) 3D model b) amplitude response

Equivalent microwave circuit of the third-order bandstop filter is shown in Fig. 11a, and fully corresponds to the 3D EM model of the filter. In the presented circuit, losses are not taken into account. Values of the elements of the circuit are calculated using equation (1). Comparison of the amplitude responses for the 3D EM model and the equivalent microwave circuit is presented in Fig. 11b. A good agreement between the results is observed in terms of the center frequency and the obtained bandwidth.

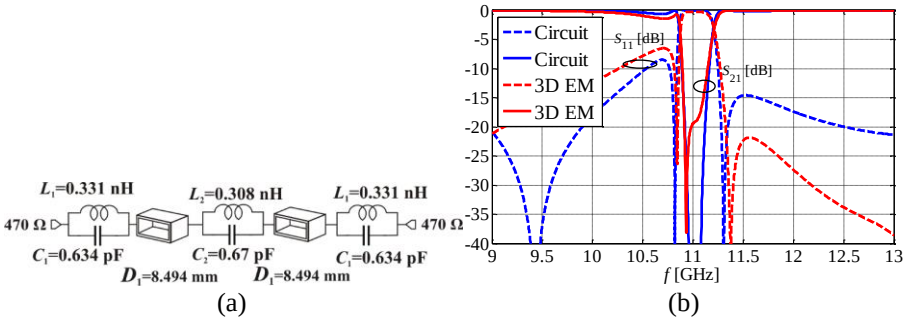


**Fig. 11** a) Equivalent microwave circuit of the *H*-plane bandstop filter.
b) Comparison of the amplitude responses for the 3D EM model and the equivalent microwave circuit

### *2.2.3. Third-order dual-band bandstop filter using SRRs*

To verify the usefulness of the design, a third-order *H*-plane dual-band bandstop filter is proposed for the center frequencies $f_{01}$ = 9 GHz and $f_{02}$ = 11 GHz [11, 12]. 3D model of the filter is shown in Fig. 12a. SRRs for different stopbands are separated by the quarter-wavelength waveguide sections to realize the immittance inverters for the corresponding center frequency. So, designed stopbands can be controlled independently. SRRs for the different stopbands are distanced by $(\lambda_{g9GHz} - \lambda_{g11GHz})/4$ = 3.678 mm.

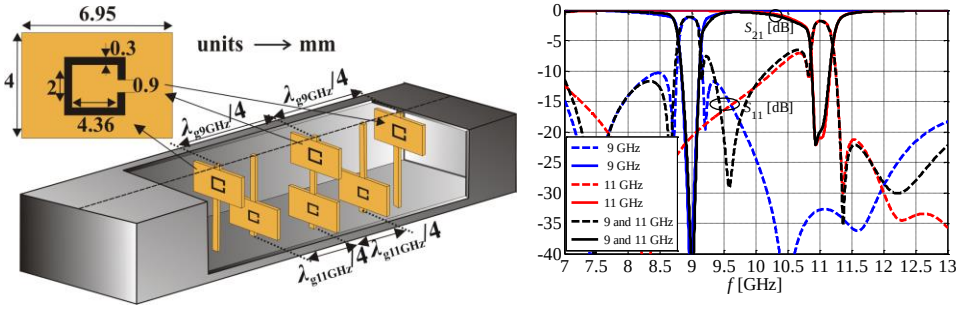


**Fig. 12** *H*-plane dual-band bandstop filter: a) 3D model b) amplitude response

## 3. BANDPASS FILTER DESIGN

Bandpass waveguide filters can be designed using inserts with different types of resonators. The inserts may be placed in the *E*-plane or *H*-plane of the rectangular waveguide. Herein, bandpass waveguide filters using *H*-plane inserts with CSRRs as resonating elements, are considered. In fact, as relatively simple resonators to model and fabricate, providing bandpass frequency response, CSRRs are widely used for bandpass waveguide filter design. They allow us to control the frequency response by modifying their parameters, thus providing flexible design. Some of the previously reported solutions can be found in the open literature. In [21], the use of CSRR for the *H*-plane bandpass design is demonstrated. A third order bandpass filter using CSRRs is presented in [22], while compact solution can be found in [23].

### 3.1. Resonating inserts with CSRRs

Resonating insert with CSRR, placed in the *H*-plane of the standard rectangular waveguide (WR-90), is assumed to be a basic element of the higher-order filters. Therefore, various implementations of the waveguide resonators with such inserts are possible. First, waveguide resonator using multi-layer planar insert with CSRR is shown in Fig. 13a. Substrate used for the printed-circuit insert is copper-clad polytetrafluoroethylene (PTFE)/woven glass laminate (TLX-8) (http://www.taconic-add.com). The parameters of this substrate are as follows: $\varepsilon_r = 2.55$, $\tan\delta = 0.0019$, $h = 1.143$ mm and $t = 18$ μm. The specification of this resonator requires a resonant frequency of $f_0 = 11.1$ GHz and a 3-dB bandwidth of $B_{3dB} = 520$ MHz. The equivalent microwave circuit of the waveguide resonator is also given in Fig. 13a. The following equations [6, 24] are used for calculation of the circuit parameters:

$$R = Z_0 \frac{|S_{21}(j\omega_0)|}{2(1-|S_{21}(j\omega_0)|)},\ L = B_{3dB} Z_0 \frac{|S_{21}(j\omega_0)|}{2\omega_0^2},\ C = \frac{2}{B_{3dB} Z_0 |S_{21}(j\omega_0)|}, \tag{3}$$

where $\omega_0$ denotes the angular frequency in (rad/s), $B_{3dB}$ is 3dB bandwidth (rad/s), $S_{21}(j\omega_0)$ is the value of the $S_{21}$ parameter at the considered resonant frequency. The impedances of ports correspond to the value of the wave impedance of the waveguide for the resonant frequency of $f_0 = 11.1$ GHz (468 Ω).

As shown in Fig. 13b, the amplitude response meets given specification, for the chosen CSRR dimensions. Also, there is a god agreement of the obtained amplitude responses of the 3D EM model and equivalent circuit. The printed-circuit insert presented here used basic CSRR form; however, CSRR may have additional elements for the amplitude response fine-tuning, as exemplified in [24, 25].

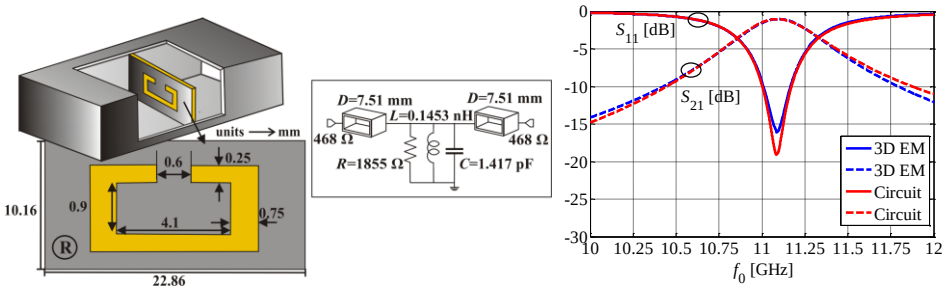


(a) (b)

**Fig. 13** Waveguide resonator using multi-layer planar insert with CSRR: a) 3D model and equivalent microwave circuit, b) comparison of amplitude responses

Besides multi-layer planar structures, the resonating insert can be a pure metallic structure, which is even easier to implement (Fig. 14a). The thickness of the metal insert is 100 μm. The conductivity of the metal plates is set to σ = 20 MS/m to include the losses (the surface roughness and the skin effect). This resonator achieves resonant frequency of $f_0$ = 11.06 GHz (Fig. 14b).

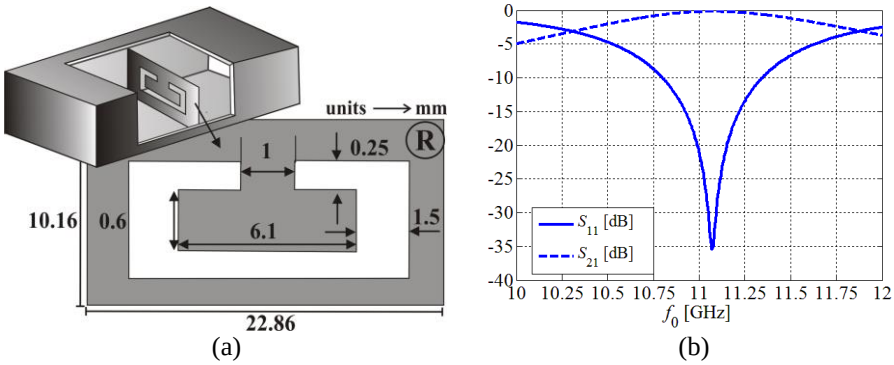


(a) (b)

**Fig. 14** Waveguide resonator using metal insert with CSRR: a) 3D model, b) amplitude response

In the previously considered models, CSRR was centrally positioned on the insert. However, this is not mandatory; in fact, by changing the position of the resonator (besides modifying its parameters) one can influence the frequency response.

Relatively simple design of the waveguide resonator using metal insert with CSRR-like resonator attached to the top waveguide wall [26] is depicted in Fig. 15a. The

obtained amplitude response, having bandpass characteristic, is shown in Fig. 15b ($f_0$ = 11.06 GHz, $B_{3dB}$ = 680 MHz). Similarly, resonator can be attached to the bottom waveguide wall.

A common property of all presented types of inserts is that more than one resonator can be accommodated on the insert, thus allowing for multiple resonant frequencies. In fact, by properly positioning the resonators, each frequency band can be independently tuned, by modifying parameters of a single resonator. This is an important property for the multi-band filter design. Some of the previously reported printed-circuit discontinuities with multiple resonant frequencies can be found in [3, 6, 24, 26-28].

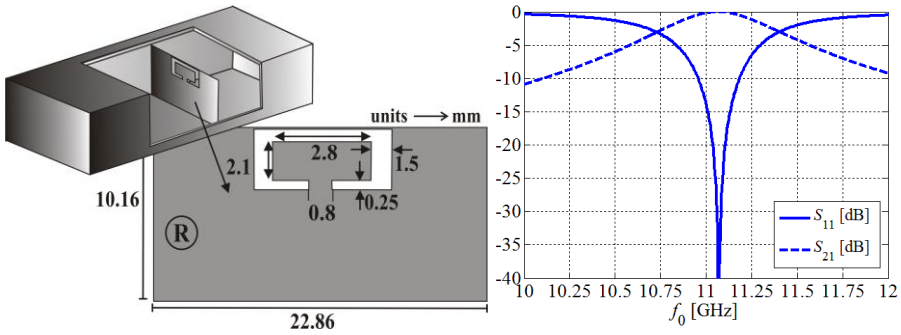


(a) (b)

**Fig. 15** Waveguide resonator using metal insert with CSRR:
a) 3D model, b) amplitude response

### 3.2. Third-order filter using CSRRs

Starting from the printed-circuit insert with CSRR, higher-order filter can be designed. Since the resonating circuits are connected in parallel, inverters are needed between them [4, 29]. For the waveguide filter design, an inverter can be deployed as a quarter-wave waveguide section at the center frequency of interest, as explained in [3, 6].

A third-order bandpass filter, with a single pass band, is considered as an example of the higher-order filter design. It uses multi-layer planar inserts with CSRRs of the same substrate as the insert shown in Fig. 13a. The 3D model of the filter is shown in Fig. 16a. Filter is designed to meet the following specification: $f_0$ = 11 GHz, $B_{3dB}$ = 300 MHz. Therefore, the parameters of the CSRRs are set to achieve that. Also, the waveguide sections of length equal to $\lambda_{g\ 11GHz}/4$ = 8.49 mm represent inverters between the resonating elements. Fig. 16b shows the obtained amplitude response.

### 3.3. Multi-band bandpass filter design

As previously stated, resonating inserts with multiple resonant frequencies can be used for the higher-order multi-band filter design. However, it is necessary to properly design the inserts and the inverters, as well. This means that each waveguide section representing inverter has to be of the proper length equal to $\lambda_g/4$ ($\lambda_g$ is guided wavelength in the waveguide), for each center frequency. Therefore, the folded inserts have been introduced

as an adequate solution [3, 6, 25, 27, 28], being a novel solution at the same time, compared to the available open literature.

To exemplify the use of the folded inserts for the filter design, a second-order dual-band ($f_{01}$ = 9 GHz, $f_{02}$ = 11 GHz) filter model with two multi-layer planar inserts is shown in Fig. 17a. As can be seen, the parts of the inserts with CSRRs are mutually separated for the proper distance to meet the invertor requirement and the fold is achieved by adding a metal plate to connect these parts. The substrate used for the inserts is RT/Duroid 5880 ($\varepsilon_r$ = 2.2, $h$ = 0.8 mm) (http://www.rogerscorp.com). According to Fig. 17a, the lengths of the inverters are $\lambda_{g\,9GHz}/4$ = 12.17 mm and $\lambda_{g\,11GHz}/4$ = 8.49 mm and the metal plate length is $l_{pl} = (\lambda_{g\,9GHz} - \lambda_{g\,11GHz})/8$ = 1.84 mm. For the insert designated as I1, the width of the metal plate corresponds to the waveguide width. The other possibility is to have narrow plate connecting the resonating inserts (insert I2). In the considered example, the width of the metal plate is set to $w_{pl}$ = 3 mm. The obtained amplitude responses for the filters having both inserts implemented as I1 or I2 (with the same dimensions and positions of the CSRRs) are compared in Fig. 17b. As can be seen, for the model with I2 inserts, a transmission zero occurs above the upper band. Since dimensions of the CSRRs have not been tuned for the I2 insert, the discrepancy between the parameters of the frequency bands is notable; however, the idea is to present the design possibilities and to point at their influence.

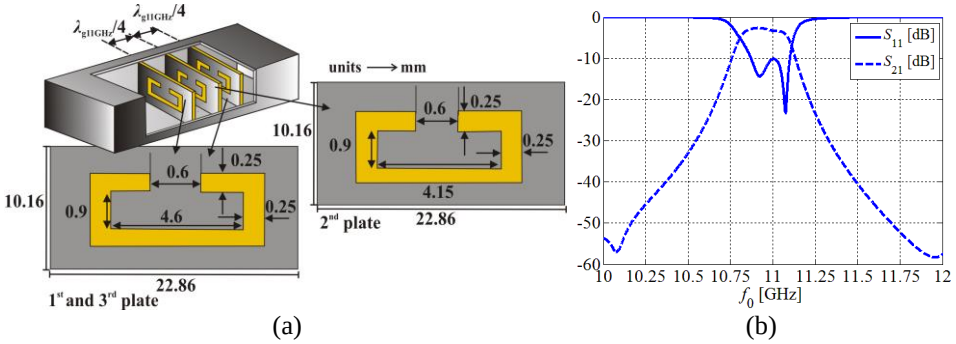


(a) (b)

**Fig. 16** Third-order bandpass filter using multi-layer planar inserts with CSRRs: a) 3D model, b) amplitude response

The previous model may be simplified by using metal inserts [27, 28], instead of the multi-layer planar ones (Fig. 18a). The filter is designed to meet the following specification: $f_{01}$ = 9 GHz, $B_{3dB\text{-}1}$ = 450 MHz, $f_{02}$ = 11 GHz, $B_{3dB\text{-}2}$ = 650 MHz. Regarding the inverter implementation, the same stands as for the filter in Fig. 17a. Therefore, the distances between the resonators are $\lambda_{g\,9GHz}/4$ = 12.17 mm and $\lambda_{g\,11GHz}/4$ = 8.49 mm. The length of the metal plate of the folded insert is $l_{pl} = (\lambda_{g\,9GHz} - \lambda_{g\,11GHz})/8$ = 1.84 mm. An equivalent microwave circuit has been generated for this filter in NI AWR Microwave Office (http://www.awrcorp.com) (Fig. 18b). Each resonating insert is represented by a network consisting of *RLC* circuits (for each CSRR) and an inductor connected between them. The inverter is represented by a waveguide section of length equal to $\lambda_{g\,9GHz}/4$, inserted between these networks. The details regarding equivalent microwave circuit and the equations used for calculation of the lumped elements parameters can be found in [3, 6, 25, 27, 28].

Comparison of the amplitude responses obtained by a 3D EM simulation and an equivalent circuit is given in Fig. 18c.

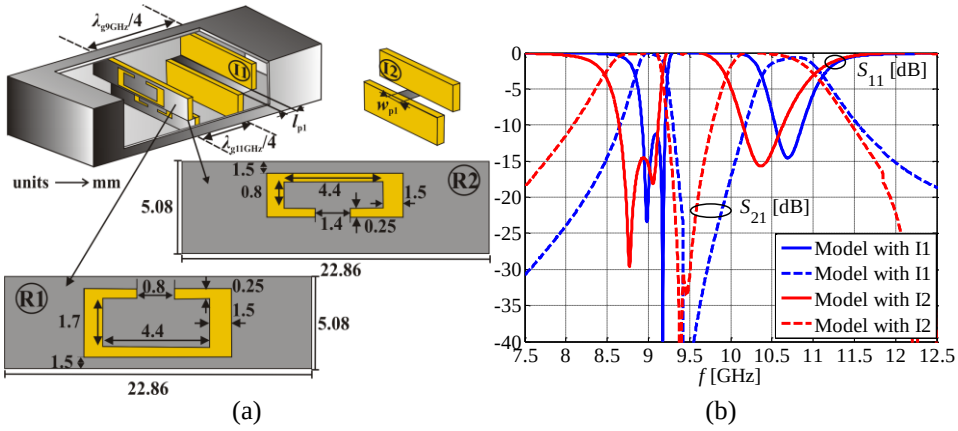


**Fig. 17** Second-order dual-band bandpass filter using multi-layer planar inserts with CSRRs: a) 3D model, b) amplitude responses

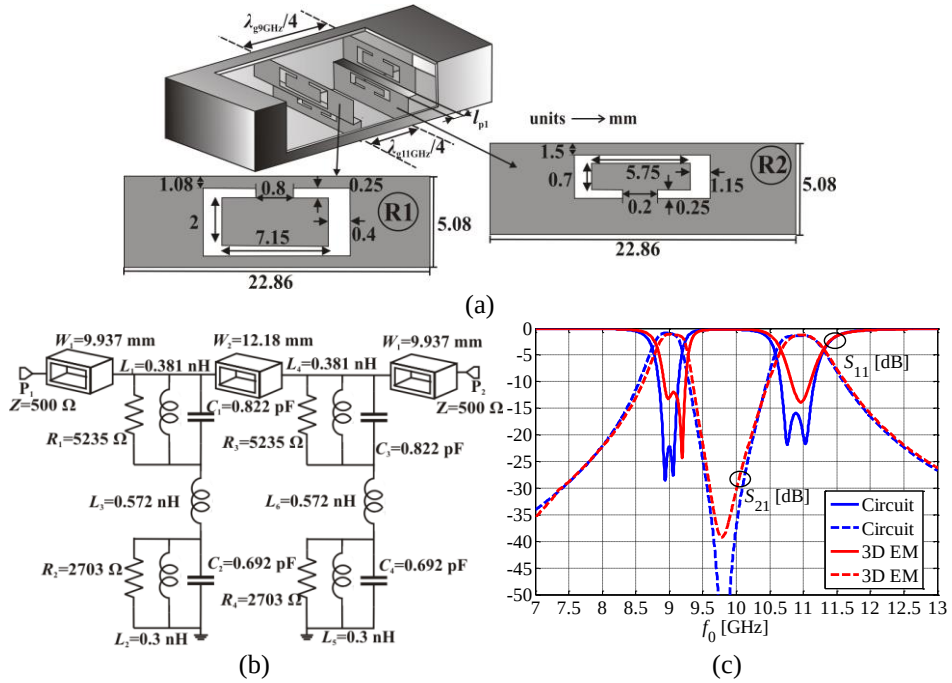


**Fig. 18** Second-order dual-band bandpass filter using metal inserts with CSRRs: a) 3D model, b) equivalent microwave circuit, c) comparison of amplitude responses

In order to develop a compact filter, the waveguide sections representing inverters may be shortened; however, an additional properly designed insert between the resonating inserts is needed to preserve the original filter response. This way of miniaturization assumes that the normalized lengths of the inverters are the same for both center frequencies, but the resonating inserts are still folded. For the sake of easier fabrication, a solution with flat inserts has been proposed, as more optimal one [3, 6, 25, 28] (Fig. 19a). As can be seen, the additional insert is still needed; however the inverters for the center frequencies are not miniaturized in the same manner (the normalized length of the inverter for the CSRRs with $f_{01}$ = 9 GHz is $\lambda_{g\,9GHz}/8$, while the normalized length of the inverter for the CSRRs with $f_{02}$ = 11 GHz is equal to $0.18\lambda_{g\,11GHz}$). Fig. 19b shows comparison of amplitude responses before and after applying inverter miniaturization, with the same and different normalized lengths of the inverters, for the considered second-order dual-band filter.

Fabrication of the flat metal inserts is relatively simple; however, supporting plates and fixtures are needed in order to have stable inserts inside the waveguide [6, 30]. In [3, 28] a detailed explanation regarding filter fabrication can be found, including the implementation of the structure for precise positioning of inserts. The proposed solution has been successfully deployed for the experimental verification and the measured results have shown good agreement with the simulated ones.

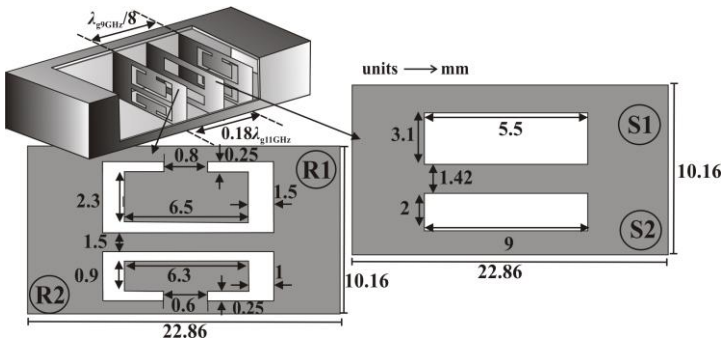


(a)

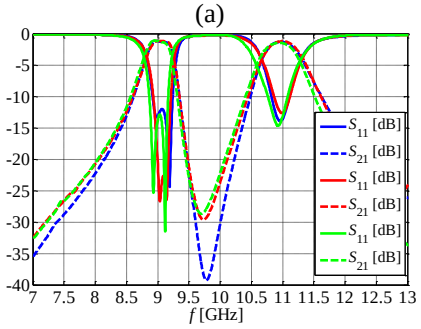


(b)

**Fig. 19** Compact second-order dual-band bandpass filter using flat metal inserts: a) 3D model, b) comparison of amplitude responses of the filter without inverter miniaturization (blue), with equal (red) and unequal (green) inverter miniaturization

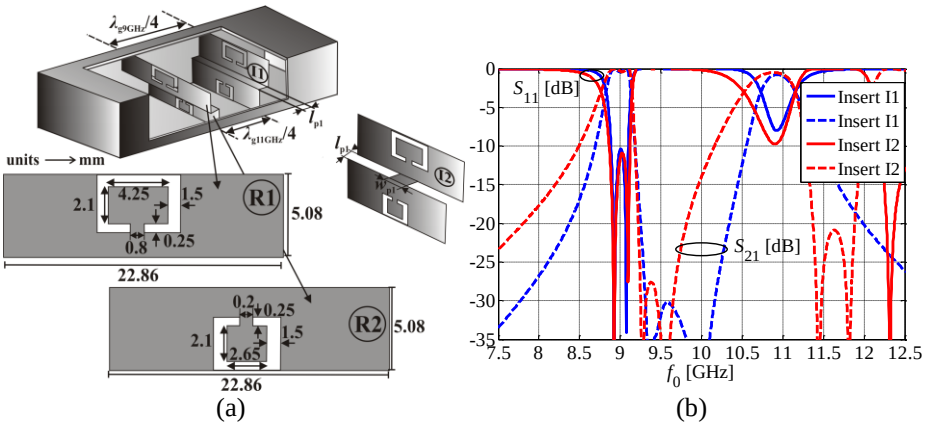


(a) (b)

**Fig. 20** Second-order dual-band bandpass filter using metal inserts with CSRRs attached to the waveguide walls: a) 3D model, b) amplitude responses

Multi-band filters may be also designed using inserts with resonators attached to the waveguide walls, as an example with a single resonator shown in Fig. 15a. A second order dual-band filter, with two folded metal inserts, is shown in Fig. 20a [26]. Dimensions of the resonators are tuned to provide center frequencies of $f_{01}$ = 9 GHz and $f_{02}$ = 11 GHz. Therefore, the lengths of the inverters are $\lambda_{g\,9GHz}/4$ = 12.17 mm and $\lambda_{g\,11GHz}/4$ = 8.49 mm and the metal plate length is $l_{pl} = (\lambda_{g\,9GHz} - \lambda_{g\,11GHz})/8$ = 1.84 mm. Proposed resonators occupy less space on the insert, compared to the centrally positioned CSRRs, for the same resonant frequencies (the occupied area may be reduced up to 20 %). For the insert designated as I1, the width of the metal plate corresponds to the waveguide width. The other possibility is to have narrow plate connecting the resonating inserts (insert I2). In the considered example, the width of the metal plate is set to $w_{pl}$ = 2 mm. The obtained amplitude responses for the filters having both inserts implemented as I1 or I2 (with the same dimensions and positions of the resonators) are compared in Fig. 20b. As can be seen, for the model with I2 inserts, a transmission zero occurs above the upper band and better matching is obtained for that band, as well; however, at the expense of the wider band.

## 4. BANDPASS WAVEGUIDE FILTER FABRICATION SIDE EFFECTS

An important step of the filter design procedure is certainly experimental verification, i.e. the measurement of the filter response on a fabricated prototype. At that point, obtained simulation models may be optimized and corrected and another control fabrication may be performed [31]. Fabrication process itself may affect the obtained filter responses; thus a study of imperfections should be carried out in order to estimate the influence of the fabrication side effects on the amplitude response.

This topic has already gained attention, since some previously published papers considered the influence of the substrate parameters on the frequency response of the microwave structures (e.g. [32]). Regarding waveguide filters fabrication and possible deviations of the frequency response, some of the available solutions can be found in [33-38].

In our study, we have considered various implementation imperfections and fabrication side effects influencing the frequency response of the bandpass waveguide filters [31]. Since these filters use printed-circuit inserts as discontinuities, we have taken into account the parameters of the substrate (dielectric permittivity, thickness, losses, including the tolerances) used for the multi-layer planar inserts. Furthermore, a machine used for fabrication may introduce some inaccuracy and imperfections during the fabrication of the inserts. Finally, it is not always possible to have stable and perfectly positioned inserts in the waveguide during the measurement and regular operation, so this should be also taken into account when investigating filter response deviation. Our goal was to investigate the influence of the aforementioned imperfections on the bandpass waveguide filter amplitude response by making precise 3D EM models, which included considered effects, and by performing software simulations. In this manner, we were able to estimate the influence of various effects and phenomena on the filter response and make conclusions regarding the most relevant ones. Also, the advantage of this method of investigation is the fact that majority of settings can be made in software, without unnecessary fabrications, thus shortening filter design procedure. The experimental verification of the chosen models has confirmed simulated results, showing good mutual agreement, thus confirming the proposed method for investigation, as well.

We have considered a waveguide resonator using single CSRR (Fig. 13a) and a third-order filter, as a more complex structure using three multi-layer planar inserts with CSRRs (Fig. 16a). In both cases, substrate used for the inserts is copper-clad polytetrafluoroethylene (PTFE)/woven glass laminate (TLX-8), with the following nominal values of the substrate parameters and the tolerances: $\varepsilon_r = 2.55 \pm 0.04$, $\tan\delta = 0.0019 \pm 0.001$, $h = 1.143 \pm 0.05715$ mm, $t = 18$ μm (http://www.taconic-add.com/). The conductivity of the metal plates was set to $\sigma = 20$ MS/m to include the losses (the surface roughness and the skin effect).

For the modeling of the waveguide structures, WIPL-D software has been used (http://www.wipl-d.com/), to make precise models with various effects included and to perform full-wave simulations of metallic and dielectric structures [39]. For the printed-circuit inserts fabrication, a MITS Electronics FP21-TP machine (http://www.mitspcb.com/) has been used. According to the manufacturer's specification, precision of the machine can be specified as follows: a minimum achievable microstrip line width is 50 μm and a minimum gap between microstrip lines is 50 μm. CSRRs have been made using milling process. All filter response measurements have been performed on the Agilent N5227A network analyzer.

In order to be able to investigate the influence of the considered effects and phenomena, we have analyzed the filter response deviation. In fact, this deviation could be qualified as a difference between the nominal value of the observed parameter of the amplitude response (center frequency, bandwidth, insertion loss) and the value obtained when some of the fabrication side effects are taken into account. Furthermore, the deviation could be quantified by a relative change of the parameters of the amplitude response [31],

$$x_{rel}\,[\%] = 100(x - x_{ref})/x_{ref}, \tag{4}$$

where $x_{rel}$ is the relative change in percent, $x$ represents the obtained value and $x_{ref}$ is the reference (nominal) value, without introducing any inaccuracy. Accordingly, an absolute change could be calculated as $x_{abs} = x - x_{ref}$.

We have adopted a set of criteria to evaluate performance degradation. Therefore, we have assumed that the filter response is not significantly degraded if the following conditions are met: 1) the relative change of the center frequency ($f_{0rel}$) is less than 1 %, 2) the relative change of the bandwidth ($B_{3dBrel}$) is less than 2 %, 3) the absolute change of the passband attenuation ($S_{21abs}(f_0)$) is less than 0.3 dB. The filter response degradation was analyzed and evaluated using simulation results of the 3D EM models and measurement results on the laboratory prototype.

### 4.1. Influence of the design parameters

In order to investigate the influence of the implementation technology, the substrate parameters have been varied according to the manufacturer's specification provided earlier in this section. The same procedure has been carried out for the waveguide resonator and the third-order filter. In the latter case, it has been assumed that each printed-circuit insert was made using the same substrate board, thus the same type of imperfection was applied to all inserts. The substrate parameters $\varepsilon_r$, tan $\delta$ and $h$ have been varied discretely, within the provided boundaries, and the frequency response parameters ($f_{0rel}$, $B_{3dBrel}$, $S_{21abs}(f_0)$) have been observed. A complete set of the obtained numerical results can be found in [31]. While the change of tan $\delta$ and $h$ practically had no influence, the most significant degradation of the amplitude response has been introduced by varying $\varepsilon_r$ ($f_{0rel}$ was nearly 0.5 %, $B_{3dBrel}$ was below 2 % and $S_{21abs}(f_0)$ was significantly lower than 0.3 dB, related to the reference values), for both the waveguide resonator and the filter. Since the given criteria have been met, one can conclude that the variation of the substrate parameters within the tolerances provided by the manufacturer, does not introduce significant degradation of the amplitude response. Fig. 21 shows comparison of amplitude responses for various values of $\varepsilon_r$.

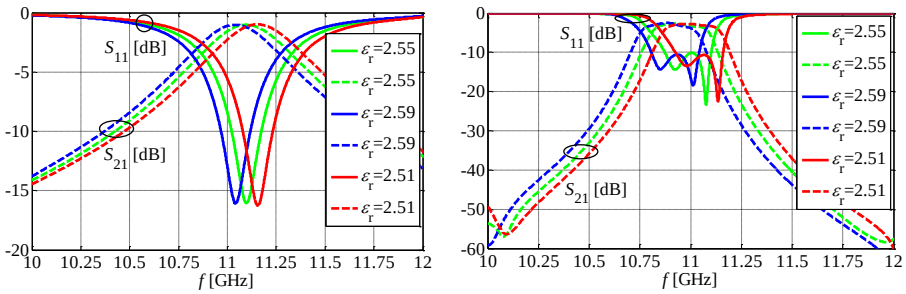


**Fig. 21** Comparison of amplitude responses for various values of $\varepsilon_r$: a) waveguide resonator, b) waveguide filter

Since the relative dielectric permittivity had the most significant influence on the amplitude response, the next step in our study was to find analytical expression of the resonant frequency ($f_0$) in terms of $\varepsilon_r$. Therefore, we have analyzed the amplitude response for various values of $\varepsilon_r$ in case only one printed-circuit insert was placed in the waveguide (the first/third insert or the second insert of the filter) and in case of the third-order filter.

The obtained results have shown that there is a linear dependency between $f_0$ and $\varepsilon_r$, in the following form [31]:

$$f_0 = k\,\varepsilon_r + m, \tag{5}$$

where $k = 1.43$ and $m$ varies. This expression represents the best linear fit to each set of the obtained results (Fig. 22). In practice, for the desired resonant frequency, one should perform a measurement using single insert, and based on that and the given family of curves, the exact permittivity can be determined and used for the filter design.

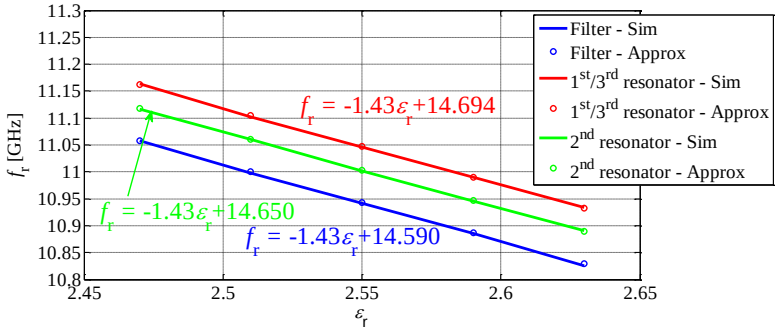


**Fig. 22** Design curve: resonant frequency as a linear function of permittivity

### 4.2. Inaccuracy of the machine used for fabrication

The machine used for fabrication of the printed-circuit inserts may also introduce some inaccuracy, thus the obtained amplitude response may be degraded to some extent. We have considered a few possible issues related to the machine tolerance.

As previously mentioned, the milling process was used to remove the metallization. Therefore, it was possible to obtain traces, i.e. CSRRs, with larger or smaller dimensions than those given in the design specification. The details of the analysis and the obtained simulation results are given in [31]. It has been shown that the amplitude response does not get degraded in case the deviation of the trace width is within the limits of ± 5 μm.

The next considered issue is also a consequence of using the milling process. Namely, while removing the metallization, the tool may dig into the substrate to a certain depth [40]. In our study, a trace of cylindrical tool was used and the 3D EM model of such insert was successfully made in WIPL-D software [31]. Fig. 23 shows compared amplitude responses for various values of the digging depth $d$, for the waveguide resonator and the third-order filter. As can be seen, by increasing the depth, the center frequency increases, as well, and the bandwidth gets wider, for both the waveguide resonator and the filter. For the waveguide resonator, there is a good agreement of the simulated and measured results for $d = 50$ μm (Fig. 23a), thus confirming the proposed method for modeling the influence of this type of inaccuracy in the software. In addition, the following conclusions can be made: 1) for a single insert, the digging depth of 10 μm can be declared as critical; 2) for the filter using three inserts with the same digging depth, critical value is even lower than 10 μm (which is around 50 % of the metallization thickness).

Finally, we have considered the possibility to fabricate inserts with dimensions not exactly the same as those of the waveguide cross-section. In our example, the insert was narrowed by the same amount on both sides. The detailed analysis and the simulated and measured results can be found in [31]. It has been confirmed that this effect practically does not have influence on the amplitude response (for both waveguide resonator and filter), despite the fact that the insert was not physically short-circuited to each waveguide wall. Precisely, in case the inserts were equally narrowed, by the same amount, on both sides, this amount should be kept below 500 μm (i.e., 1000 μm in total), so the filter response does not get degraded.

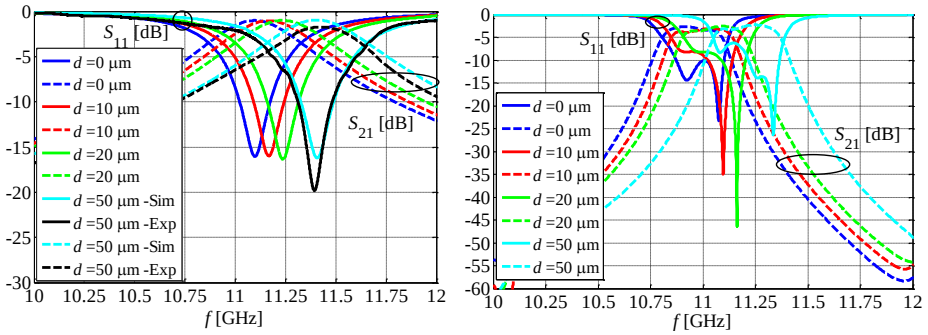


**Fig. 23** Comparison of amplitude responses for various values of digging depth *d*:
a) waveguide resonator (including measurement results for $d$ = 50 μm),
b) waveguide filter

### 4.3. Precise positioning of inserts

The inaccuracy in positioning of printed-circuit inserts might introduce filter response degradation. Therefore, we have considered two possible issues – inclined and rotated inserts – for both waveguide resonator and filter. The detailed analysis has been carried out for a single insert, and those results have been further taken into account when considering positioning of inserts for the third-order filter.

Fig. 24a shows an inclined insert in the waveguide and two possible situations from the practice were considered. In case the dimensions of the fabricated insert perfectly match the dimensions of the waveguide cross-section ($b_1 = b$), the following equation can be used to calculate the inclination angle [31]:

$$\cos(\alpha) = b/(b+x),\ \ x = 2bw^2/(b^2 - w^2)\,. \tag{6}$$

It has been shown that the critical angle which still allows the insert to remain more or less stable, i.e. to have contact with the top and bottom waveguide walls, is $\alpha \approx 13^{\circ}$. The other possible situation is to have the insert fabricated to be shorter than needed ($b_1 \neq b$). The inclination angle that still provides stable insert, for known value of $b_1$, can be calculated using following equation [31]:

$$\cos(\alpha) = b/(b_1+x),\ \ x = (b_1 w^2 \mp wb\sqrt{w^2 + b_1^2 - b^2})/(b^2 - w^2)\,. \tag{7}$$

In case of shorter insert, the critical inclination angle may have lower values (e.g. $\alpha = 4^o$), compared to the case with $b_1 = b$.

Furthermore, Fig. 24b shows a rotated insert in the waveguide and the minimum rotation angle can be found using following equation [31]:

$$\cos(\theta) = (a/2)/(a/2 + x), \quad x = aw^2/(a^2 - w^2). \tag{8}$$

The minimum rotation angle for the insert with dimensions perfectly matching the waveguide cross-section is $\theta \approx 6^o$. The maximum rotation angle (in positive or negative direction) which does not introduce response degradation is $\theta = 15^o$. It has been shown, that in this case the insert has physical contact with the waveguide walls over its top and bottom sides, so it should remain stable although it is not perfectly short-circuited to the side walls [31].

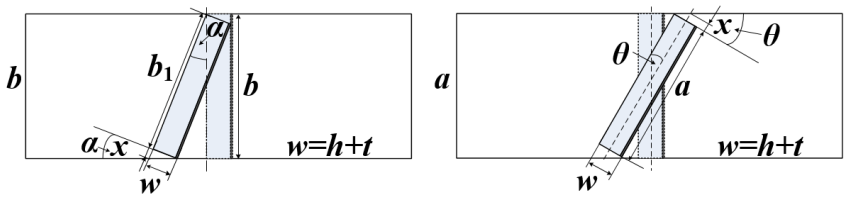


**Fig. 24** Printed-circuit insert in the waveguide:
a) inclined by α (side view), b) rotated by θ (top view)

In case a single insert is inclined by $\alpha = 13.038^o$ or rotated by $\theta = 15^o$, it has been shown that there is no significant influence on the amplitude response of the waveguide resonator [31].

The next step was to investigate the influence of the inaccurately positioned inserts on the third-order filter response. In this case, the function of the inverters may be disrupted, since their lengths may be inadequate. Therefore, we have thoroughly investigated the filter response in case one or multiple inserts were rotated or inclined.

We have considered the filter with the central insert rotated by $\theta = 15^o$ (Fig. 25a) and it has been shown that this type of inaccuracy does not introduce significant amplitude response degradation, particularly in the passband (Fig. 25b). Fabricated filter is shown in Fig. 25c. The detailed explanation regarding filter fabrication along with the structures designed to hold the inserts can be found in [30, 31]. A comparison of the simulated and measured amplitude responses shows their good agreement, as can be seen in Fig. 25d.

Finally, the amplitude response has been analyzed when two or three inserts were inclined or rotated, since these are also possible situations in practice. It has been shown that cases with all three inclined or rotated inserts exhibit the most significant response degradation, so these models were considered in details in [31], and herein the most important observations will be pointed out. In case of three inclined inserts, Fig. 26a shows models with the most noticeable performance degradation. Namely, model 1 results in the most significant response deviation, even for small inclination angles. However, model 2 is the most probable one in practice: in case the fixtures holding the inserts, attached to the top and bottom waveguide walls, are mutually shifted, all three

inserts are inclined by the same angle, in the same direction. For the model 2 with perfectly fabricated inserts and inclination angle $\alpha \approx 13^{o}$, $B_{3dBrel}$ is around 5 %, compared with the reference bandwidth of the original filter. For the same model with slightly shorter inserts ($b_1 \approx 10.1$ mm) and inclination angle $\alpha = 8^{o}$ for all three inserts, practically there is no response degradation, i.e. the parameters of the amplitude characteristic met the criteria provided earlier in this section. In case of three rotated inserts, model 1 in Fig. 26b exhibited the most significant response deviation. It has been found that the maximum rotation angle, still providing acceptable amplitude response in terms of required criteria for an arbitrary position of the inserts, was $\theta = 8^{o}$. Finally, in case the inserts were simultaneously inclined and rotated, the aforementioned criteria would be met for the inclination angle $\alpha \leq 5^{o}$ and the rotation angle $\theta \leq 7^{o}$.

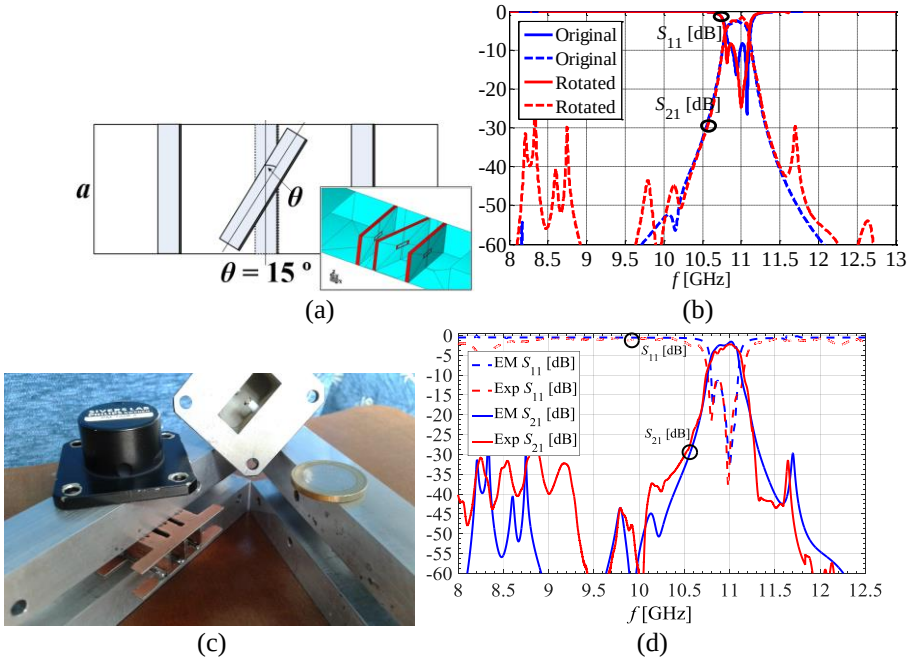


**Fig. 25** Filter with central insert rotated by $\theta = 15^{o}$: a) top view and WIPL-D model, b) comparison of amplitude responses for the original model and filter with rotated insert, c) fabricated filter, d) comparison of simulated and measured results for the filter with rotated insert

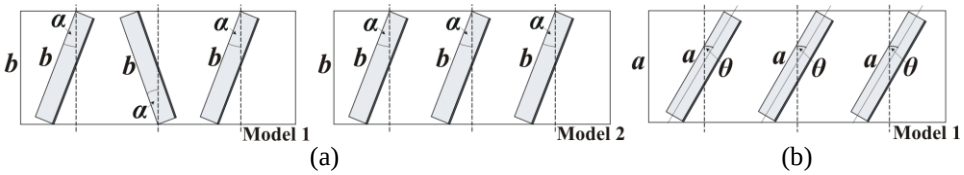


**Fig. 26** a) Inclined inserts, b) rotated inserts

## 5. CONCLUSIONS

In this paper, various solutions for the bandstop and bandpass waveguide filter design have been presented. The goal was to exemplify the method for relatively simple waveguide filter design procedure, using printed-circuit discontinuities and different types of resonators, easy to design and implement.

First, bandstop filters were designed using printed-circuit inserts within the rectangular waveguide. Inserts with SRRs were placed in the *H*-plane, while the insert with QWRs was positioned in the *E*-plane of the standard WR-90 waveguide. Designed filters using these inserts have been thoroughly analyzed and the results have been presented. Both types of the considered filters allow independent control of the designed stopbands and are compact in size.

As for the *E*-plane filters, miniaturized ICDS multi-band bandstop waveguide filter design using QWRs has been discussed. As a proof of concept, *E*-plane ICDS dual-band and triple-band bandstop waveguide filters have been designed. Center frequencies can be flexibly adjusted by the length of the corresponding QWRs. As for the ICDS dual-band bandstop filter, connection of the QWRs for different stopbands to the opposite waveguide walls has resulted in about 41 % of the size reduction, compared to the case where they are connected to the same waveguide wall. Miniaturized ICDS dual-band bandstop filter has been fabricated and measured. The filter is 0.512 $\lambda_g$ in length. Further miniaturization of the dual-band bandstop filter has been achieved when QWRs of different size were printed one below another. In this arrangement, the unwanted mutual coupling has been particularly strong and restricted the control of the center frequencies and bandwidth. The impact of the physical dimensions alteration on the filter response has been thoroughly investigated and exposed. Obtained ultra-compact *E*-plane dual-band bandstop waveguide filter has length of 0.295 $\lambda_g$, which is about 66 % and 42 % shorter compared to the non-miniaturized and miniaturized ICDS dual-band bandstop filter, respectively. Additionally, equivalent microwave circuit of the multi-band bandstop filter with independently tunable stopbands is presented in the form of a cascade of the equivalent microwave networks of the single-band bandstop filters. Equivalent circuit corresponds to the decomposed 3D filter structure, and it is suitable for faster filter design and optimization, as well.

For the design of the *H*-plane filters, inserts with printed SRRs have been used. The third-order bandstop filter has been designed using SRRs distanced by the quarter-wave waveguide sections acting as immittance inverters for the center frequency. Accordingly, dual-band bandstop filter has been implemented with SRRs separated by the inverters for the specified center frequencies. The filter is 0.5 $\lambda_g$ in length, which is attributed to the length of the quarter-wave waveguide section used as inverter for lower stopband design.

Regarding bandpass waveguide filters, various types of resonating inserts, having bandpass characteristic, have been introduced. They have been used for the higher-order *H*-plane bandpass filters with a single or multiple pass bands. A novel solution for dual-band filter using folded inserts has been presented, in order to properly implement the inverters, i.e. the quarter-wave waveguide sections, for each center frequency. The inserts may be implemented either as multi-layer planar inserts or metal inserts, as a simpler solution. Dual-band filter with folded metal inserts has been further modified to obtain compact solution with flat inserts and miniaturized inverters, optimized for fabrication. It has been also demonstrated that CSRRs do not necessarily need to be centrally positioned on the inserts, but they may be attached to the top and bottom waveguide walls.

Finally, the bandpass waveguide filters fabrication side effects have been investigated in details. The amplitude responses of the waveguide resonator and the third order filter have been analyzed in terms of the implementation technology, the tolerance of the machine used for fabrication and positioning of the inserts inside the waveguide. The obtained results are relevant for identifying critical parameters affecting the performance of the considered structures. Various effects and phenomena have been modeled in software and for the chosen examples the results were also experimentally verified, showing good agreement with the simulation results. The obtained results can be summarized as follows: 1) regarding substrate parameters, the dielectric permittivity of the printed-circuit insert had the major impact on the amplitude response (a closed-form expression based on a linear dependency between the permittivity and center frequency was proposed as a design curve); 2) in terms of machine tolerance, the digging depth into the substrate during the milling process introduced the most significant response degradation; 3) the inaccuracy in positioning of the inserts in the waveguide did not introduce deviation of the filter response in the passband, for the critical angles which were determined, for both the waveguide resonator and the filter with three arbitrarily inclined or rotated inserts.

The findings of our study may be applicable for the other types of waveguide filters using similar resonating inserts and also for the filters operating in different frequency bands, since the presented results pointed out the most significant phenomena and side effects of the fabrication process.

The advantage of the proposed method is the possibility for improving and shortening the design procedure, by performing majority of setting and analyses in the software, thus avoiding unnecessary fabrications.

**Acknowledgement:** *This work was supported by the Ministry of Education, Science and Technological Development of the Republic of Serbia under Grant TR32005.*

## REFERENCES

[1] M. D. Lutovac, D. V. Tošić, B. V. Evans, *Filter Design for Signal Processing using MATLAB and Mathematica*, Upper Saddle River, NJ: Prentice Hall; Translated in Chinese. Beijing, P. R. China: Publishing House of Electronics Industry, PHEI; 2004.

[2] D. M. Pozar, *Microwave engineering*. New York: John Wiley & Sons, 2012.

[3] S. Stefanovski Pajović, M. Potrebić, D. V. Tošić, "*Advanced Filtering Waveguide Components for Microwave Systems*", Microwave Systems and Applications, Dr. Sotirios Goudos (Ed.), InTech, January 2017.

[4] R. J. Cameron, C. M. Kudsia, and R. R. Mansour, *Microwave Filters for Communication Systems: Fundamentals, Design and Applications*, New Jersey: John Wiley & Sons, 2007.

[5] B. Milovanović, J. Joković, T. Dimitrijević, "Analysis of Feed Waveguide Length Influence on EM Field in Microwave Applicator Using TLM Method", *Facta Universitatis, Series: Electronics and Energetics*, vol. 21, no.1, pp. 65-72, April 2008.

[6] S. Lj. Stefanovski, "*Microwave Waveguide Filters Using Printed-Circuit Discontinuities*", Ph.D. dissertation, School of Electrical Engineering, University of Belgrade, Belgrade, Serbia, 2015.

[7] S. C. Dutta Roy, "A New Lumped Element Bridged-T Absorptive Band-Stop Filter", *Facta Universitatis, Series: Electronics and Energetics*, vol. 30, no. 2, pp. 179-185, June 2017.

[8] S. Prikolotin, A. Kirilenko, "A Novel Notch Waveguide Filter", *Microw. Opt. Techn. Let.*, vol. 52, pp. 416-420, February 2010.

[9] S. Fallahzadeh, H. Bahrami, M. Tayarani, "A Novel Dual-Band Bandstop Waveguide Filter Using Split Ring Resonators", *Prog. Electromagn. Res. Lett.*, vol. 12, pp. 133-139, 2009.

[10] S. Fallahzadeh, H. Bahrami, M. Tayarani, "Very Compact Bandstop Waveguide Filters Using Split Ring Resonators and Perturbed Quarter-Wave Transformers", *Electromagnetics*, vol. 30, no. 5, pp. 482-490, June 2010.

[11] S. Stefanovski, M. Potrebić, D. Tošić, "Novel Realization of Bandstop Waveguide Filters", *Technics*, special edition, pp. 69-76, 2013.

[12] S. Stefanovski, M. Potrebić, D. Tošić, "A Novel Design of Dual-Band Bandstop Waveguide Filter Using Split Ring Resonators", *J. Optoelectron. Adv. Mat.*, vol. 16, no. 3-4, pp. 486-493, March-April 2014.

[13] S. Stefanovski, M. Potrebić, D. Tošić, Z. Cvetković, "Design and Analysis of Bandstop Waveguide Filters Using Split Ring Resonators", In Proceedings of the 11th International Conference on Applied Electromagnetics (PES 2013), Niš, Serbia, 2013, pp. 135-136.

[14] M. Mrvić, M. Potrebić, D. Tošić, Z. Cvetković, "*E*-plane Microwave Resonator for Realisation of Waveguide Filters", In Proceedings of XII International SAUM Conference on Systems, Automatic Control and Measurements (SAUM 2014), Niš, Serbia, 2014, pp. 205–208.

[15] S. Stefanovski Pajović, M. Potrebić, D. Tošić, Z. Stamenković, "*E*-plane Waveguide Bandstop Filter With Double-Sided Printed-Circuit Insert", *Facta Universitatis, Series: Electronics and Energetics*, vol. 30, no. 2, pp. 223-234, June 2017.

[16] H. Sun, C. Feng, Y. Huang, R. Wen, J. Li, W. Chen, G. Wen, "Dual-Band Notch Filter Based on Twist Split Ring Resonators", *Int. J. Antennas Propag.*, vol. 2014, Article ID 541264, 6 pages, April 2014.

[17] P. Castro, J. Barosso, J. Leite Neto, A. Tomaz, U. Hasar, "Experimental Study of Transmission and Reflection Characteristics of a Gradient Array of Metamaterial Split-Ring Resonators", *J. Microw., Optoelectron. Electromagn. Appl.*, vol. 15, no. 4, pp. 380-389, October/December 2016.

[18] S. Stefanovski, M. Potrebić, D. Tošić, "A Novel Design of *E*-Plane Bandstop Waveguide Filter Using Quarter-Wave Resonators", *Optoelectron. Adv. Mat.*, vol. 9, no. 1-2, pp. 87-93, January-February 2015.

[19] M. Mrvić, M. Potrebić, D. Tošić, "Compact *E*-Plane Waveguide Filter with Multiple Stopbands", *Radio Sci.*, vol. 51, no. 12, pp. 1895-1904.

[20] M. Mrvić, M. Potrebić, D. Tošić, Z. Cvetković, "Miniaturization of Waveguide Bandstop Filter", In Proceedings of the 12th International Conference on Applied Electromagnetics (PES 2015), Niš, Serbia, 2015, pp. 79–80.

[21] N. Ortiz, J. D. Baena, M. Beruete, F. Falcone, M. A. G. Laso, T. Lopetegi, R. Marques, F. Martin, J. Garcia-Garcia, M. Sorolla, "Complementary Split-Ring Resonator for Compact Waveguide Filter Design", *Microw. Opt. Techn. Let.*, vol. 46, no. 1, pp. 88-92, July 2005.

[22] M. M. Potrebić, D. V. Tošić, Z. Ž. Cvetković, N. Radosavljević, "WIPL-D Modeling and Results for Waveguide Filters with Printed-Circuit Inserts", In Proceedings of the 28th International Conference on Microelectronics (MIEL 2012), Niš, Serbia, 2012, pp. 309-312.

[23] H. Bahrami, M. Hakkak, A. Pirhadi, "Analysis and Design of Highly Compact Bandpass Waveguide Filter Utilizing Complementary Split Ring Resonators (CSRR)", *Prog. Electromagn. Res.*, vol. 80, pp. 107-122, 2008.

[24] S. Stefanovski, M. Potrebić, D. Tošić, "Design and Analysis of Bandpass Waveguide Filters Using Novel Complementary Split Ring Resonators", In Proceedings of the 11th International Conference on Telecommunications in Modern Satellite, Cable and Broadcasting Services (TELSIKS 2013), Niš, Serbia, 2013, pp. 257-260.

[25] S. Stefanovski Pajović, M. Potrebić, D. Tošić, "Microwave Bandpass and Bandstop Waveguide Filters Using Printed-Circuit Discontinuities", In Proceedings of the 23rd Telecommunications Forum (TELFOR 2015), Belgrade, Serbia, 2015, pp. 520-527.

[26] S. Stefanovski, Đ. Mirković, M. Potrebić, D. Tošić, "Novel Design of H-Plane Bandpass Waveguide Filters Using Complementary Split Ring Resonators", In Proceedings of Progress In Electromagnetics Research Symposium (PIERS 2014), Guangzhou, China, 2014, pp. 1963-1968.

[27] S. Stefanovski, M. Potrebić, D. Tošić, Z. Stamenković, "A Novel Compact Dual-Band Bandpass Waveguide Filter", in Proceedings of IEEE 18th International Symposium on Design and Diagnostics of Electronic Circuits and Systems (DDECS 2015), Belgrade, Serbia, 2015, pp. 51-56.

[28] S. Stefanovski, M. Potrebić, D. Tošić, Z. Stamenković, "Compact Dual-band Bandpass Waveguide Filter with *H*-plane Inserts", *J. Circuit Syst. Comp.*, vol. 25, no. 3, 1640015 (18 pages), 2016.

[29] J.-S. Hong, Microstrip filters for RF/microwave applications, NJ: John Wiley & Sons, 2011.

[30] S. Stefanovski, M. Potrebić, D. Tošić, "Structure for Precise Positioning of Inserts in Waveguide Filters", in Proceedings of the 21st Telecommunications Forum (TELFOR 2013), Belgrade, Serbia, 2013, pp. 689-692.

[31] S. Lj. Stefanovski Pajović, M. M. Potrebić, D. V. Tošić, Z. Ž. Cvetković, "Fabrication Parameters Affecting Implementation of Waveguide Bandpass Filter with Complementary Split-ring Resonators", *J. Comput. Electron.*, vol. 15, no. 4, pp. 1462-1472, 2016.

[32] S. C. Gao, L. W. Li, T. S. Yeo, M. S. Leong, "A Dual-frequency Compact Microstrip Patch Antenna", *Radio Sci.*, vol. 36, no. 6, pp. 1669–1682, November-December 2011.

[33] M. Albooyeh, A. A. Lotfi Neyestanak, B. Mirzapour, "Wideband dual posts waveguide band pass filter", *Int. J. Microw. Opt. Techn.*, vol. 2, no. 3, pp.203-209, 2007.

[34] N. S. Choi, D. H. Kim, G. Jeung, J. G. Park, J. K. Byun, "Design optimization of waveguide filters using continuum design sensitivity analysis", *IEEE T. Magn.*, vol. 46, no. 8, pp.2771-2774, 2010.

[35] R. L. Villaroya, "*E-Plane Parallel Coupled Resonators for Waveguide Bandpass Filter Applications*", Ph.D. dissertation, Heriot-Watt University, Edinburgh, 2012.

[36] [online] http://www.ros.hw.ac.uk/bitstream/handle/10399/2604/Lopez-VillarroyaR_1012_eps.pdf?sequence=1&isAllowed=y

[37] P. Soto, D. de Llanos, V. E. Boria, E. Tarin, B. Gimeno, A. Onoro, L. Hidalgo, M. J. Padilla, "Performance analysis and comparison of symmetrical and asymmetrical configurations of evanescent mode ridge waveguide filters", *Radio Sci.*, vol. 44, no. 6, RS6010, December 2009.

[38] J. Bornemann, J. Uher, "Design of Waveguide Filters Without Tuning Elements for Production-efficient Fabrication by Milling", In Proceedings of Asia-Pacific Microwave Conference (APMC), pp.759-762, Taipei, Taiwan, 2001.

[39] C. Zhao, T. Kaufmann, Y. Zhu, C. C. Lim, "Efficient Approaches to Eliminate Influence Caused by Micro-machining in Fabricating *H*-plane Iris Band-pass Filters", in Proceedings of Asia-Pacific Microwave Conference (APMC), pp.1306-1308, Sendai, Japan, 2014.

[40] B. M. Kolundžija and A. R. Djordjević, *Electromagnetic modeling of composite metallic and dielectric structures*, 1st ed. Norwood, MA: Artech House, 2002.

[41] A. R. Djordjević, D. I. Olćan, A. G. Zajić, "Modeling and design of milled microwave printed circuit boards", *Microw. Opt. Technol. Let.*, vol. 53, no. 2, pp. 264–270, 2011.